Role of lithium in enhancing radiation tolerance under γ-irradiation in lithium borosilicate waste glasses

BLACK, Aine G., EDGE, Ruth, SCRIMSHIRE, Alex <http://orcid.org/0000-0002-6828-3620>, MOHAPATRA, Manoj, BINGHAM, Paul <http://orcid.org/0000-0001-6017-0798>, BROOKFIELD, Adam, SHANMUGAM, Muralidharan, LEAY, Laura, HARRISON, Mike T., BLANC, Frédéric and PATEL, Maulik K.

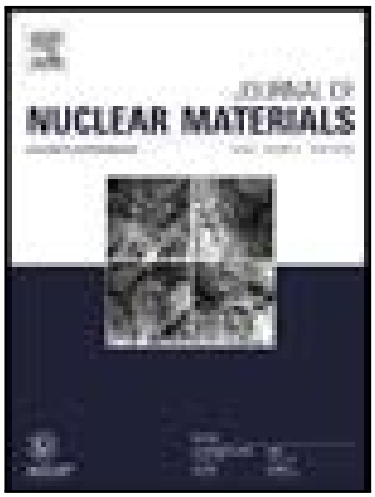

Role of lithium in enhancing radiation tolerance under γ-irradiation in lithium borosilicate waste glasses

Aine G. Black , Ruth Edge , Alex Scrimshire , Manoj Mohapatra , Paul A. Bingham , Adam Brookfield , Muralidharan Shanmugam , Laura Leay , Mike T. Harrison , Frédéric Blanc , Maulik K. Patel

PII: S0022-3115(25)00353-8
DOI: https://doi.org/10.1016/j.jnucmat.2025.155959
Reference: NUMA 155959

To appear in: *Journal of Nuclear Materials*

Received date: 20 January 2025
Revised date: 28 May 2025
Accepted date: 3 June 2025

Please cite this article as: Aine G. Black , Ruth Edge , Alex Scrimshire , Manoj Mohapatra , Paul A. Bingham , Adam Brookfield , Muralidharan Shanmugam , Laura Leay , Mike T. Harrison , Frédéric Blanc , Maulik K. Patel , Role of lithium in enhancing radiation tolerance under γ-irradiation in lithium borosilicate waste glasses, *Journal of Nuclear Materials* (2025), doi: https://doi.org/10.1016/j.jnucmat.2025.155959

Role of lithium in enhancing radiation tolerance under γ-irradiation in lithium borosilicate waste glasses

Aine G. Black[a,b], Ruth Edge[c], Alex Scrimshire[d], Manoj Mohapatra[e], Paul A. Bingham[d], Adam Brookfield[f], Muralidharan Shanmugam[f], Laura Leay[a,g], Mike T. Harrison[h], Frédéric Blanc[b,i,j*] and Maulik K. Patel[a*]*

[a]Department of Materials, Design and Manufacturing, University of Liverpool, Liverpool, L69 3GH, UK

[b]Department of Chemistry, University of Liverpool, Liverpool, L69 7ZD, UK

[c]Dalton Cumbrian Facility, University of Manchester, Westlakes Science Park, Cumbria, CA24 2HA, UK

[d]Materials and Engineering Research Institute, College of Business, Technology and Engineering, Sheffield Hallam University, Sheffield, S1 1WB, UK

[e]Radiochemistry Division, Bhabha Atomic Research Centre, Trombay, Mumbai, 400085, India

[f]Department of Chemistry and Photon Science Institute, The University of Manchester, Manchester, M13 9PL, UK

[g]United Kingdom National Nuclear Laboratory, Workington Laboratory, Havelock Road, Workington, Cumbria, CA14 3YQ, UK

[h]United Kingdom National Nuclear Laboratory, Central Laboratory, Sellafield, Cumbria, CA20 1PG, UK

[i]Stephenson Institute for Renewable Energy, University of Liverpool, Liverpool, L69 7ZF, UK

[j]Leverhulme Research Centre for Functional Materials Design, University of Liverpool, Liverpool, L7 3NY, UK

Abstract

Lithium-containing borosilicate glasses are used for the safe containment of high-level nuclear waste in the UK. Glasses were fabricated with varying Li_2O contents and irradiated to a total γ-dose of 80 MGy to probe the relationship between Li_2O contents and γ irradiation-induced defects. Semi-quantitative X-band Electron Paramagnetic Resonance (EPR) measurements revealed the formation of boron-oxygen hole centres (BOHC), electron-trap centres, Oxy radicals and hole centres (HC_1) defects after γ-radiation. The results highlight the beneficial impact lithium has on the glass network against the formation of paramagnetic defects by transforming BO_3 sites to $[BO_4]^-$. Experimental evidence from EPR and Nuclear Magnetic Resonance (NMR) spectroscopy indicated that the primary defects formed in the 4-component and 7-component glasses are BOHCs on bridging oxygens of the BO_3 sites and Oxy radicals linked to silicon atoms, respectively. All glass compositions reached defect saturation around 25 MGy suggesting that the number of components in the glass network or Li_2O content does not significantly influence saturation dose, however, no change in the environment or connectivity of the boron, sodium or silicon subnetworks was observed by multinuclear NMR.

1. Introduction

Vitrification is the process of immobilising High-Level radioactive Waste (HLW) in a durable solid matrix where the radioactive elements are chemically bonded into the glass structure [1]. The main sources of radiation in HLW for the first 100 years will be from fission products, such as ^{90}Sr and ^{137}Cs, which are short lived β-emitters, and subsequently from long lived α-emitting minor actinides, such as ^{241}Am and ^{244}Cm [2]. β-decay results in the emission of γ-rays which will interact with the glass through ionisation resulting in the formation of defects such as electron trap centres [3,4] and hole centres [5,6] in the glass network. Conversely, damage by α-emitting minor actinides is predominantly *via* displacive damage from recoil atoms and ionization from helium atoms from the α-decay. In this work, we explore the effect of γ-rays on the modifications in multicomponent borosilicate glasses.

The glass compositions used for the immobilisation of HLW are typically alkali borosilicate glasses; however, the optimum composition differs depending on the composition of the country's HLW stream [7]. In the UK, lithium-containing borosilicate glass compositions are used and termed 'Mixture Windscale' (MW) a 4-oxide glass, and 'Calcium Zinc' (CaZn) a 7-oxide glass.

Lithium is of interest due to its broad application across many fields such as, lithium-ion batteries [8,9], ionic glasses [10,11] and nuclear waste storage [2,12]. Lithium ions are small, highly mobile and have a large Cation Field Strength (CFS). Lithium can have two roles in the glass network simultaneously, *i.e.* as network modifier or charge compensator. The most recent study characterising the MW and CaZn glass networks assessed the impact lithium content has on the connectivity of the two glass networks [13]. It was found that an increase in lithium content resulted in an increase in $[BO_4]^-$ sites at the expense of BO_3, depolymerisation of the silicate network and a reduction in the glass transition temperature. It was also discovered that lithium had a greater impact on the stability of the glass network in CaZn, compared to MW, as the CaZn network experienced a greater change in connectivity at higher lithium contents. The use of ^{11}B and ^{6}Li Nuclear Magnetic Resonance (NMR) spectroscopy employing dipolar-coupling and J-coupling Heteronuclear Multiple Quantum Correlation (D-HMQC [14] and J-HMQC [15]) experiments enabled the authors to probe through space (D-HMQC) or through bond (J-HMQC) correlations. The authors demonstrated that Li^+ ions are in close proximity to BO_3 sites at all lithium

concentrations but only at higher lithium contents are Li^+ ions near $[BO_4]^-$ sites where they act as charge compensator. ^{11}B Magic Angle Spinning (MAS) NMR spectra revealed that non-bridging oxygens (NBO) do not exist on the BO_3 sites in any of the MW and CaZn glass compositions targeted. The same glass compositions have been used in this work to assess the impact of lithium content on the formation of γ-radiation induced defects.

The effect of ionising radiation on the MW glass composition has been investigated in the past using γ-radiation doses up to 10 MGy [16–18]. These studies used Electron Paramagnetic Resonance (EPR) spectroscopy to confirm the presence of paramagnetic defects, atoms or ions possessing at least one unpaired electron such as Boron Oxygen Hole Centre (BOHC), Electron Trapped centres (ET and E'), Oxy radicals and Hole Centres (HC). However, no significant structural or mechanical property changes were observed *via* Raman spectroscopy or Vickers hardness testing, respectively. To the best of our knowledge, only two γ-radiation studies have been carried out on the 7-oxide CaZn glass and uncertainty remains in the assignment of all paramagnetic species formed after γ-irradiation [16,19]. This is likely because its multicomponent composition produces EPR spectra that are broad and difficult to deconvolute making defect assignment challenging. Furthermore, despite these glasses being intended for the storage of HLW in a Geological Disposal Facility (GDF) for over 10,000 years, the current literature on these glass compositions only go up to 10 MGy of γ-radiation doses, equivalent to ~ 10 years of storage time [18,20]. Here we detail, *via* semi-quantitative EPR measurements, the effect of γ-radiation on the MW and CaZn glass networks when saturated with paramagnetic defects and identify that this occurs at a γ-irradiation dose of ~ 25 MGy for all glass compositions in this work. Additionally, the impact this defect saturation dose of ~ 25 MGy has on the ^{11}B, ^{23}Na and ^{29}Si NMR spectra is explored. It is important to understand the role that the composition has in the defect formation as it determines where in the network the defects form. It is understood that these glass compositions do not contain NBOs on the BO_3 sites therefore we strongly infer, with supporting evidence from NMR and EPR spectroscopies, that the BOHCs formed in these glasses are all on bridging oxygens (BOs) in the boron network.

2. Materials and Methods

2.1 Sample preparation

The glass frit, supplied by the United Kingdom National Nuclear Laboratory (UKNNL), contains half of the final amount of lithium as half is held back in the vitrification process in order to be re-added with the liquid HLW feed as $LiNO_3$ where it acts as a flux to optimise calcination [21,22]. The full lithium glasses were prepared by adding the appropriate quantity of Li_2CO_3 (a laboratory substitute for $LiNO_3$) to the respective frits. The glasses are termed MW ½Li, MW full-Li, CaZn ½Li and CaZn full-Li throughout this work. Full sample preparation details and compositional analysis are given in our previous publication [13] and all samples were powdered prior to γ-irradiation. The measured compositions by Inductively Coupled Plasma Optical Emission Spectrometry (ICP-OES) and X-Ray Fluorescence (XRF) Spectrometry are tabulated in Table 1.

Table 1: Glass compositions as measured by ICP-OES for B and Li and XRF for all remaining oxides in oxide mol% [13]. The uncertainty noted in the measured values is for the cation. The presence of Fe_2O_3 in the MW full-Li glass is likely from impurities in the raw materials and is not typically present in the MW base glass.

Oxide Mol %	SiO_2	B_2O_3	Li_2O	Na_2O	Al_2O_3	CaO	ZnO	Fe_2O_3
MW ½Li	65.27 ± 1.51	19.32 ± 0.60	4.56 ± 0.09	10.73 ± 0.41	0.13 ± 0.01	-	-	-
MW full-Li	60.08 ± 1.42	20.27 ± 0.64	9.35 ± 0.18	9.98 ± 0.39	0.25 ± 0.01	-	-	0.15 ± 0.01
CaZn ½Li	53.29 ± 1.18	20.35 ± 0.60	2.20 ± 0.04	8.24 ± 0.30	2.98 ± 0.13	7.61 ± 0.24	5.32 ± 0.27	-
CaZn full-Li	49.34 ± 1.10	21.62 ± 0.65	5.53 ± 0.10	7.67 ± 0.28	3.64 ± 0.16	7.23 ± 0.23	4.97 ± 0.26	-

2.2 γ-irradiations

The γ-irradiations were performed using a Foss Therapy Services 812 ^{60}Co Gamma irradiator at the Dalton Cumbrian Facility, The University of Manchester, which supplies 1.17 and 1.33 MeV energy γ-photons from three ^{60}Co source rods with activity evenly distributed along each rod, supplying a planar radiation field [2,3]. Glass powders were contained in clear glass vials in a two-tiered sample holder (Figure S1). The glass powders remained in the same position throughout the duration of the studies.

The samples were placed the same distance from the ^{60}Co source and received the same rate of irradiation. Approximately 60 g of glass powder was loaded into the glass vials initially and periodically approximately 10 g of each powder was removed for analysis once the desired dose rate had been reached. The powdered glasses were irradiated to total doses of 0.5, 5, 25 and 80 MGy. The absorbed dose rates of each sample were determined using a Radcal Corporation Accu-Dose+ base unit equipped with an ion chamber, model name 10 x 6-0.18. This base unit and ion chamber are calibrated together annually to traceable UK and international standards. The chamber temperature increases over the first 45-60 minutes with a maximum measured temperature of 318 K with a new ^{60}Co source, the maximum temperature then drops over time as the source decays and a new maximum temperature of 308 K is reached. For NMR and EPR experiments, no further handling of the samples occurred, and data collection was carried out within a month after the desired dose rate had been reached. The irradiated samples remained in a secured desiccator before measurements were carried out. Additional details on the ^{60}Co γ-irradiator at the Dalton Cumbrian Facility, University of Manchester are given in [2,3].

2.3 Electron Paramagnetic Resonance

First derivative continuous wave EPR spectra were obtained for all glass compositions and doses at room temperature and at the X-band frequency (~ 9.86 GHz) with a sweep width and central field of 1000 G and 3500 G, respectively, using a Bruker EMX Plus spectrometer with a 1.8 T electromagnet. The magnetic field modulation was 100 kHz, the microwave power 1 mW, the power attenuation 23 dB and the modulation amplitude 5 G. Additional spectra using the same parameters but with a wider sweep width of 6000 G and central field of 3000 G were acquired on a standard sample of $Cu(OAc)_2$ and unirradiated MW full-Li to fully assess the broad EPR signal due to the presence of metal ions species in these samples.

To obtain semi-quantitative EPR results, each quartz tube was marked ~ 3 cm from the bottom and weighed prior to filling with glass powder. The weight of glass powder used varied between composition and dose due an inhomogeneous particle size distribution. An appropriate standard sample of $Cu(OAc)_2$ [25] was measured under the same experimental conditions. $Cu(OAc)_2$ has a known electron spin concentration (2.06 x10^{19} spin/cm, [25]) thus enabling the approximate quantification of

its concentration in the γ-irradiated glass powders relative to $Cu(OAc)_2$ [26]. Conventional quantitative EPR utilises the total intensity of the integrated absorbance spectrum and the weight of the measured sample. The authors employed this method, which is commonly used by others [26,27]. All mentions of the approximate electron spin concentration in the γ-irradiated glasses are given as wt% of $Cu(OAc)_2$. The error in quantifying the electron spin concentration was determined by repeating the integration calculation three times per sample and a conservative 5 % error was applied on top of this to account for differences in sample height in the EPR tube, small differences in the placement of the EPR tube in the microwave cavity, the error involved in weighing the sample prior to measuring and the varying thermal stability of the defects formed at room temperature. The relative percentage of each defect in the full-Li compositions was estimated based on the simulation and by using the copper standard.

A strong pitch was used to calibrate the g-values. The exact g-values and other Hamiltonian parameters for the various radicals generated were evaluated by the SimFonia program provided by Bruker using the second derivative EPR spectra. Only the full-Li MW and CaZn 5 MGy γ-irradiated EPR spectra were used in the fitting procedure as the nature of defects formed in the glass network did not change with γ dose or lithium content.

The second derivative EPR spectra were obtained by differentiating the first derivative EPR spectra to further elucidate the complex resonance absorption signals arising due to the superimposition of resonances arising from different paramagnetic centres.

2.4 Nuclear Magnetic Resonance

The ^{11}B MAS NMR spectra were recorded at two magnetic fields: (i) 500 MHz on a Bruker Avance NEO spectrometer equipped with a 3.2 mm HX Bruker probe, tuned to ν_0 = 160.46 MHz and spun at a MAS rate of ν_r = 10 kHz, and (ii) 800 MHz Bruker NEO spectrometer equipped with a 1.9 mm HXY tri gamma Bruker probe, tuned to ν_0 = 256.71 MHz on the X channel and under an MAS rate of ν_r = 30 kHz. Samples were packed into either 1.9- or 3.2-mm zirconia Bruker rotors and spectra were collected at room temperature. Quantitative spectra were obtained from a one pulse sequence with a central transition selective pulse of duration 0.83 μs (π/6 flip angle on the solid) with a radio frequency (rf)

field amplitude of 50 kHz at 500 MHz. 1D spectra at 800 MHz were acquired using rotor-synchronised Hahn echo pulse sequence $\pi/6 - \tau - \pi/3 - \tau -$ acq with the τ delay corresponding to one rotor period. A recycle delay of 50 s (corresponding to 5 x T_1, where T_1 is the spin-lattice relaxation time) was used for all compositions of γ-irradiated samples to allow for complete longitudinal relaxation. T_1 was measured *via* a saturation recovery pulse sequence using a saturation block of 100 $\pi/2$ pulses separated by 1 ms and resulting data were fit using the equation $I(t) = I_0[1-\exp(-(t/T_1)]$ where I(t) is the magnetization at time t, I_0 the initial magnetization, t the variable delay for magnetization build up, employing the same method as our previous publication [13]. The boron background of the probe was removed by subtracting the 1D ^{11}B MAS NMR spectra of a rotor containing KBr under the exact experimental conditions as the ^{11}B MAS NMR spectra of the glasses. The experimental ^{11}B 1D MAS NMR spectra were fit in the software DMFit [28] using a second order quadrupolar line-shape for the BO_3 sites and a Gaussian distribution for the $[BO_4]^-$ sites. Spectra were fit using quadrupolar parameters which were determined experimentally *via* ^{11}B Multiple-Quantum MAS (MQMAS) experiments on the unirradiated versions of the glass powders [13], enabling the percentage of BO_3 to $[BO_4]^-$ sites in the glass networks to be obtained.

^{23}Na MAS NMR spectra were recorded on an 800 MHz Bruker NEO spectrometer with a 1.9 mm HXY Tri gamma Bruker probe tuned to ν_0 = 211.65 MHz on the X channel. Samples were packed into 1.9 mm zirconia Bruker rotors and spun at a MAS rate of 30 kHz. A one pulse sequence with a short flip angle ($\pi/6$ on the solid) of duration 1.04 μs and rf field amplitude of 40 kHz was used. A quantitative recycle delay of 10 s was used as this was found to be sufficiently long for complete longitudinal relaxation with T_1 being measured following the same approach as detailed above for ^{11}B and from a previous publication [13].

^{29}Si MAS NMR spectra were obtained on a 400 MHz Bruker Avance III HD spectrometer using a 4 mm HXY Bruker probe in double resonance mode tuned to ν_0 = 79.50 MHz. Glass powders were packed into 4 mm zirconia Bruker rotors and spun at a MAS rate of 8 kHz. Quantitative spectra were recorded using a one pulse sequence with a $\pi/2$ flip angle of duration 5 μs at a rf field amplitude of 50 kHz using a recycle delay time equal to 5 x T_1. ^{29}Si T_1s were measured using the same experimental setup as ^{11}B

detailed above and the resulting data were fit utilising the same method previously published by the group [13] employing a stretch exponential equation $I(t) = I_0[1-\exp(-(t/T_1)^{\alpha})]$ where α is the stretch exponent. α values range from 0.4 to 0.6 due to a distribution of values arising from the amorphous nature of the glasses and it is noted that γ-irradiation did not impact on this parameter.

^{11}B, ^{23}Na and ^{29}Si chemical shifts were referenced externally to the $NaBH_4$ signal at -41.4 ppm, 1 M NaCl in H_2O at 0 ppm and the M site of Q8M8 at 11.5 ppm [29]. References were also used for rf field amplitude calibrations.

3. Results

3.1 Electron Paramagnetic Resonance

3.1.1 Unirradiated glasses

Figure 1 shows the first-derivative X-band room temperature EPR spectra for unirradiated and 25 MGy γ-irradiated MW and CaZn glass powders with their full and ½Li content. A very weak EPR signal was detected in the 330 – 370 mT for all unirradiated full-Li compositions (dashed lines in Figure 1 and spectra in Figure S3) whilst no signal is observed for the unirradiated ½Li glasses (Figure S3). EPR signal integration of the absorbance spectra and normalisation by sample weight reveal a number of defects in both unirradiated full-Li glasses to be equivalent to $7x10^{-5}$ wt% of $Cu(OAc)_2$ which is considered to be negligible.

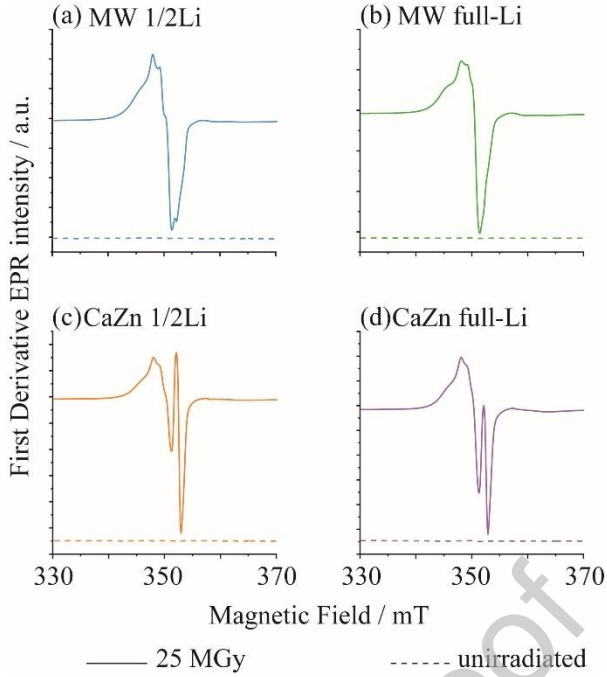

Figure 1. Experimental first-derivative X-band EPR spectra recorded at room temperature of (a) MW ½Li (blue), (b) MW full-Li (green), (c) CaZn ½Li (orange) and (d) CaZn full-Li (purple). The solid lines are the 25 MGy γ-irradiated experimental spectra that follow the same colour scheme for each composition throughout this work and the dashed lines are the experimental spectra of the unirradiated glass compositions (a magnified view of the corresponding EPR spectra is available in Figure S3), highlighting negligible defects in the latter.

3.1.2 γ-irradiated glasses

The EPR absorbance spectra comparing all four glasses are shown in Figure S2 and exhibit an asymmetrical signal around 350 mT with a small shoulder at 360 mT. The signal at 350 mT in the CaZn glass is composed up of at least two contributions, one at ~ 350 mT and ~ 355 mT. The signal at ~ 355 mT is more intense in CaZn ½Li as opposed to the full-Li implying that this signal is influenced by the lithium content of the glass network. Furthermore, as this ~ 355 mT signal is not observed in the MW compositions it infers that this signal may be related to the enhanced complexity of the CaZn network due to the additional presence of aluminium, calcium and zinc. The shoulder at 360 mT is more intense in CaZn than MW indicating that the intensity of this signal is likely composition related.

The differences between the MW and CaZn spectra are much more clearly observed in the first- (Figure 1) and second- (Figure S6) derivative EPR spectra. The first-derivative EPR spectra exhibit a sharp strong EPR resonance near g ≈ 2 (magnetic field range 330 – 370 mT) and as negligible defects were present in the unirradiated versions of the glasses in this region (Figure 1), this indicates that all defects formed in this region were created by γ-rays. The line-shape of EPR spectra of the irradiated glasses can be decomposed into a sum of several different paramagnetic defect centres as described below. In this work any change, outside of experimental error, in the unirradiated glass network after γ-irradiation is considered a defect.

There is a small variation in the EPR resonances upon lithium addition to the glass network, the EPR spectra of both ½Li MW and CaZn being slightly sharper and more intense than their full-Li counterparts. Despite this small change in line-shapes, the same EPR resonances and parameters are obtained in all EPR spectra at all γ doses, and it thus can be inferred that only the relative proportion of defects varies with lithium content whilst their nature remains the same. The defects created after γ-radiation and their corresponding three principal g-values of the g tensor were obtained from fitting the second derivative EPR spectra (Figures 2 and S6) and are detailed as follow.

Firstly, the second derivative EPR spectra of all glass compositions (Figures 2(b) and S6) revealed a well resolved quartet hyperfine splitting structure due to the presence of a BOHC in all glass compositions. A BOHC is defined as a hole trapped on an oxygen atom of a BO_3 site [4], the quartet arising from the interaction between the hole (unpaired electron) on oxygen with ^{11}B which has a spin S = 3/2 and natural abundance ~ 80 %. Coupling to ^{10}B (natural abundance ~ 20 %) with S = 3 was not observed in these glasses as, due to the low resolution and lower sensitivity, it is hidden in the linewidth of the EPR signal and buried underneath the stronger EPR signal amplitude contribution from the hyperfine coupling to ^{11}B, respectively. The magnitude of the hyperfine splitting is given by the hyperfine coupling constant A (Table 2), which depends on the nuclear moment and the size of the interaction of the unpaired electron spin density at the boron nucleus site. The size of the hyperfine splitting for a BOHC in these glasses is relatively small (~ 2 mT) indicating the unpaired electron is located away from the boron [4]. The size of A is slightly larger than reported values for other BOHCs

in the literature (~ 1.3-1.5 mT [4,30–32]) suggesting that in the MW and CaZn compositions the unpaired electron is closer to the boron inducing a larger hyperfine interaction.

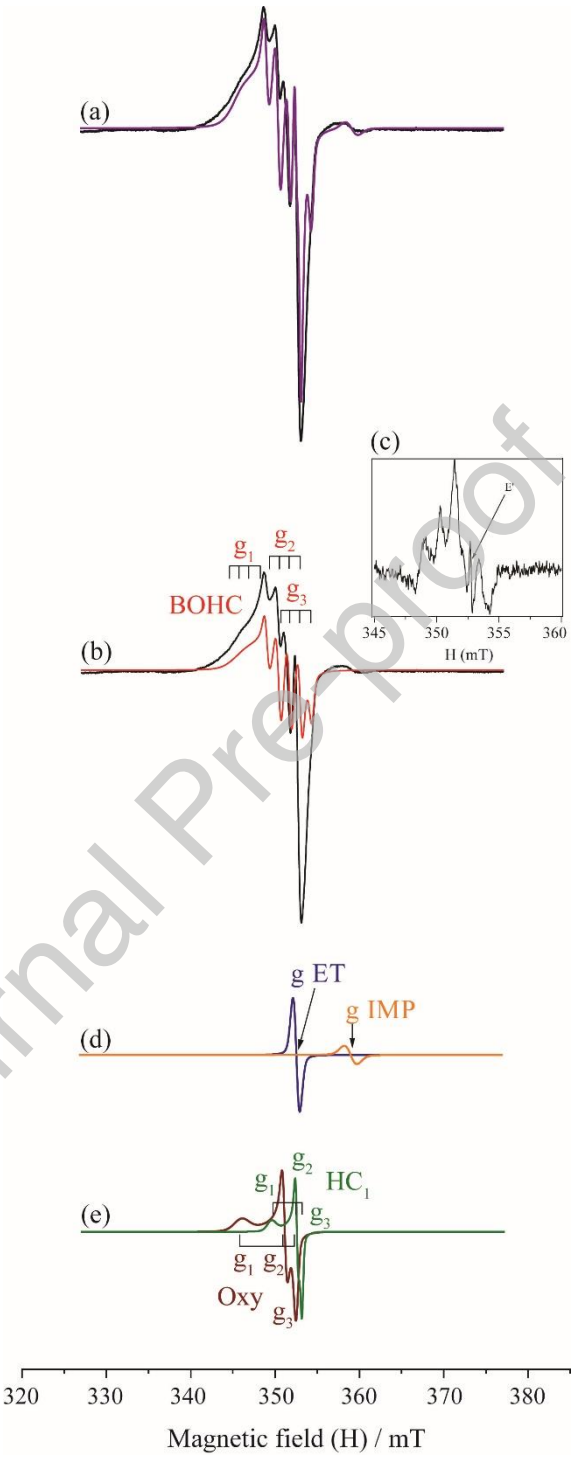

Figure 2. Room temperature experimental and simulated EPR spectra of MW full-Li irradiated to 5 MGy illustrating each defect contribution to the overall line-shape. (a) experimental (black) spectrum and simulated (purple) spectrum decomposed into (b) BOHC (red) overlaid with the experimental

spectra for comparison, (c) experimental second derivative of BOHC in MW full-Li showing the presence of the E' centre (black), (d) ET centre (blue) and impurity (IMP, yellow) and (e) Oxy centre (brown) and Hole Centre (green). The BOHC g-values are a spilt into a quartet due to coupling to ^{11}B with S= 3/2.

Secondly, an additional defect was observable in the second derivative spectra of the BOHC (inset in Figure 2(c)) and was assigned to an E' centre formed by an electron trapped on a silicon atom [4,30,33]. The corresponding EPR spectrum of this E' centre is isotropic (*i.e.*, identical principal g values $g_1 = g_2 = g_3 = 2.0015$) and is assigned to a defect with tetrahedral or octahedral symmetry [34].

A third defect with g-values g_1= 2.0022 and g_2=g_3= 2.0024 which are comparable to that of a free electron (g_0 = 2.0023) and is thus attributed to an electron self-trapped (ET, Figure 2(d)) on a cation such as Na^+, Li^+ or Ca^{2+} [3,30,35]. This ET centre is a defect possessing axial symmetry as $g_1 \neq g_2 = g_3$.

A fourth defect with g_1 = 2.0428 is present in the EPR spectra which has previously been reported to be formed due to the breaking of a peroxy linkage (≡Si-O-O-Si≡) or by the capture of a O^{2-} radical on Si Q^3 [32,36,37], this defect has been named an Oxy radical [30] (Figure 2(e)) and is also known as a Peroxy radical (POR) [17].

Finally, a fifth defect with g_1=2.0123 is observed in the EPR spectra and is known as a Hole Centre (HC) [5] (Figure 2(e)). This resonance is caused by a hole trapped on one or more oxygen atoms in the glass network. All BOHC, HC and Oxy radicals possess rhombic symmetry as $g_1 \neq g_2 \neq g_3$ [38].

The nature of defects created in the MW and CaZn glass networks upon γ-irradiation does not alter with the change in composition, however the relative proportion of each defect is dramatically different in both networks. The primary defects created in the MW glass are BOHCs (45%, Table 2) and HCs (20 %, Table 2) whereas in CaZn the primary defects are Oxy centres (35 %, Table 2) and BOHCs only make up 20 % of the defects. This explains the line-shape difference between MW and CaZn where the BOHC dominates the MW spectra and the presence of the sharp signal in the CaZn spectra is due to the dominating Oxy centre defect in this composition.

Table 2. Spin-Hamiltonian parameters obtained from fitting the second derivative experimental EPR spectra for the different defects formed after 25 MGy γ-irradiation in full-Li MW and CaZn glasses. g_i (i = 1, 2, and 3) are the individual principal g-values, A_i are the hyperfine coupling constants, Δ_i are the linewidths of the individual EPR spectra of each component and L/G is the relative Lorentzian to Gaussian ratio, all terms were obtained from simulating the experimental EPR spectra. The percentage refers to the relative percentage contribution from each defect in weight %.

Defect	g_1	g_2	g_3	A_x (mT)	A_y (mT)	A_z (mT)	Δ_x (mT)	Δ_y (mT)	Δ_z (mT)	L/G	MW %	CaZn %
BOHC	2.0346	2.0210	2.0021	1.5	2.0	2.1	1.6	0.6	0.6	0.5	45	25
Oxy	2.0428	2.0200	2.0040	-	-	-	1.5	0.6	0.5	0.2	15	35
HC	2.0123	2.0033	2.0001	-	-	-	1.0	0.4	0.3	0.2	20	15
E’	2.0015	2.0015	2.0015	-	-	-	0.25	0.25	0.25	0.5	10	10
ET	2.0022	2.0024	2.0024	-	-	-	0.75	0.75	0.75	0.2	5	10
Impurity	1.9645	1.9645	1.9645	-	-	-	0.15	0.15	0.15	0.5	5	5

The electron spin concentration of 25 MGy γ-irradiated MW ½Li (glass sample with most defects) was calculated to be ~ 0.1 wt% of the one in $Cu(OAc)_2$ [25] which is a factor of approximately 1000 larger than the electron spin concentration in the unirradiated glasses. More generally, the relationship between lithium content and defect concentration is illustrated in Figure 3. As the amount of lithium in MW and CaZn glasses is increased, the number of defects is reduced suggesting that lithium is beneficial to the glass network against the formation of paramagnetic defects. Furthermore, since CaZn has fewer defects than MW for all radiation doses excluding 80 MGy, we infer that the CaZn glass network is more stable against the formation of defects. A saturation of defects appears at ~ 25 MGy with the possible recombination and annihilation of electron-hole pairs occurring between 25-80 MGy yielding a significant decrease in defect concentration in the full-Li samples. This large decrease is not observed in their ½Li counterparts as any change in defect concentration between 25-80 MGy is within experimental error, potentially indicating there is a relationship between lithium content and defect recombination. It should be noted that the γ-radiation induced defects in glass have varying thermal stabilities [17,39,40] that will have a small impact on the electron spin quantification and the weighting of each defect at room temperature (see the experimental section 2.3 for details on error analysis).

The relationship between defect production and γ-ray dose is however not linear inferring that one γ-ray does not result in the creation of one defect. The maximum number of defects created is ~ 10^5 defects (MW ½Li) at a γ-irradiation dose of 25 MGy.

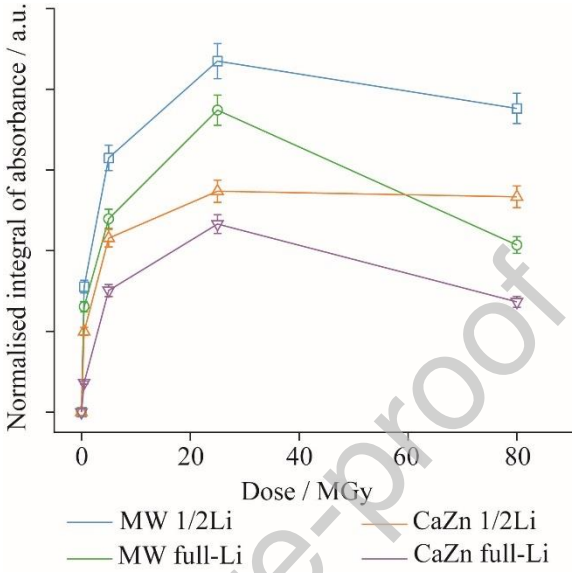

Figure 3. The integral of absorbance of the X-band EPR spectra for all γ-radiation doses in MW ½Li (blue, squares), MW full-Li (green, circles), CaZn ½Li (orange, triangles) and CaZn full-Li (purple, inverted triangles). Errors are estimated as 5 % of the integration value. The integral of absorbance has been normalised by weight of the sample.

3.2 Nuclear Magnetic Resonance

The ^{11}B MAS NMR spectra of the four glass compositions irradiated with 25 MGy γ-radiation are shown in Figure 4. In all glass compositions a γ-radiation dose of 25 MGy had the largest defect concentration (Figure 3), thus, if there is any change in the ^{11}B MAS NMR spectra, and particularly the BO_3:$[BO_4]^-$ ratio due to γ-radiation, this dose would likely have the most significant effect. The ^{11}B MAS NMR spectra of borosilicate glasses consist of two main resonance signals: a narrow resonance centered around 0 ppm attributed to boron in tetrahedral coordination ($[BO_4]^-$) and a broader resonance centered around 15 ppm attributed to boron in trigonal coordination (BO_3) [13,41]. The $[BO_4]^-$ peak is

narrower due to the symmetry of this coordination resulting in a Gaussian line-shape with a small electric field gradient and thus a small quadrupolar coupling constant (C_Q) of ~ 0.3 MHz. Contrastingly, the BO_3 peak is broad with a second order quadrupolar line-shape and a large quadrupolar coupling constant of ~ 2.8 MHz [13,42,43].

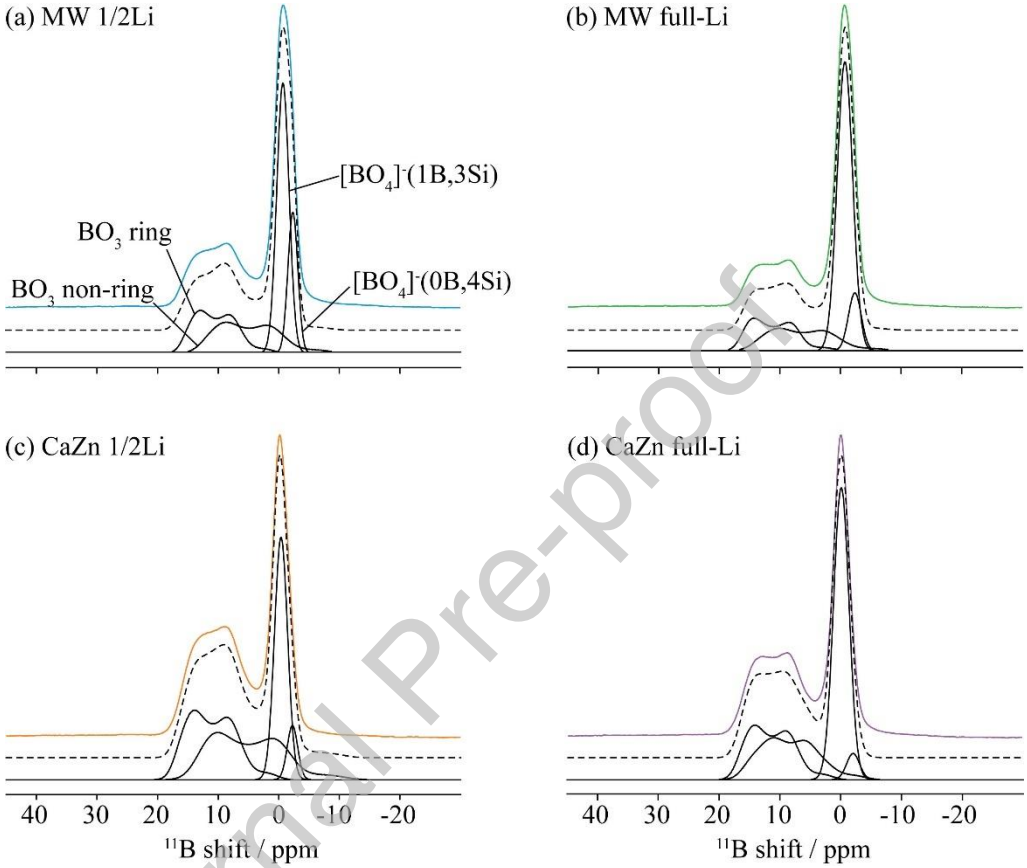

Figure 4. Deconvolution of the quantitative ^{11}B MAS NMR spectra at 500 MHz for 25 MGy γ-irradiated (a) MW ½Li (blue), (b) MW full-Li (green), (c) CaZn ½Li (orange), and (d) CaZn full-Li (purple) glasses based on ^{11}B MQMAS of the unirradiated version of the glasses published previously [13]. The coloured lines are the experimental spectra, the dashed black lines are the total fit using the appropriate models specified in section 2.4 and the BO_3 ring and non-ring and the $[BO_4]^-$(0B,4Si) and $[BO_4]^-$(1B,3Si) sites are represented by solid black lines. Only the spectra in (a) are labelled but (b-d) follow the same labelling.

Each of the two resonances consist of contributions from two different coordinations which were determined previously *via* 2D ^{11}B MQMAS NMR experiments at 400 and 500 MHz [13]. The ^{11}B

MQMAS of the BO_3 signal revealed two different BO_3 sites: one with an isotropic shift of 18 ppm and C_Q of ~ 2.6 MHz assigned to BO_3 units in ring structures and the second site with an isotropic shift of 15 ppm and C_Q of ~ 3 MHz assigned to BO_3 units in non-ring structures [13,44–46]. The ^{11}B MQMAS of the $[BO_4]^-$ species revealed at least two different sites: one with an isotropic shift of -2 ppm attributed to $[BO_4]^-$ (0B,4Si) where the central boron has four silicon next nearest neighbours, and a second site with an isotropic shift of 0 ppm assigned to $[BO_4]^-$ (1B,3Si) where the central boron has three silicon and one boron next nearest neighbours [13,46].

The ^{11}B MAS NMR spectra of the 25 MGy γ-irradiated glasses and their unirradiated counterparts are very similar (Figure 4), thus the γ-irradiated spectra were fit with the same NMR parameters extracted from the MQMAS of their unirradiated counterparts [13]. This reproduced fits in excellent agreement with the experimental spectra enabling the percentage contribution from each boron site to be obtained. Table 3 reports this data for each boron site in the 25 MGy γ-irradiated samples and in comparison with the unirradiated glasses. Within experimental error, there is no significant change in the percentage contribution from each boron site when irradiated with a dose of 25 MGy γ-radiation. There appears to be a small difference in the percentage of BO_3 and $[BO_4]^-$ sites in the CaZn full-Li sample after 25 MGy γ-radiation which has been tentatively attributed to the error associated with removing the boron background as ^{11}B MAS NMR Hahn echo spectra (where the boron background is suppressed by this experiment) at 800 MHz of the unirradiated samples. Figure S7 compares the corresponding ^{11}B MAS NMR spectra for the unirradiated and 25 MGy γ-irradiated samples highlighting identical line-shapes and thus indicating that no detectable change in boron subnetwork connectivity has occurred.

Table 3. Percentage contribution of each boron coordination in 25 MGy γ-irradiated and unirradiated powders obtained from ^{11}B MAS NMR spectra. ^{11}B NMR parameters and the percentage contribution of each boron site in the unirradiated versions of the glasses were obtained previously [13], the same model and parameters provided an excellent fit for the 25 MGy γ-irradiated glasses.

Coordination	Relative percentage in 25 MGy (± 3) / %	Relative percentage in unirradiated (± 3) / %
MW ½Li		

BO_3 ring	23	20
BO_3 non-ring	22	20
$[BO_4]^-$(0B,4Si)	16	18
$[BO_4]^-$(1B,3Si)	39	42
MW full-Li		
BO_3 ring	19	18
BO_3 non-ring	17	17
$[BO_4]^-$(0B,4Si)	9	11
$[BO_4]^-$(1B,3Si)	55	54
CaZn ½Li		
BO_3 ring	32	31
BO_3 non-ring	32	34
$[BO_4]^-$(0B,4Si)	5	7
$[BO_4]^-$(1B,3Si)	31	28
CaZn full-Li		
BO_3 ring	26	26
BO_3 non-ring	27	31
$[BO_4]^-$(0B,4Si)	3	4
$[BO_4]^-$(1B,3Si)	44	39

The EPR spectra of the γ-irradiated glasses confirmed the presence of paramagnetic centres which can potentially be correlated with the ^{11}B, ^{23}Na and ^{29}Si NMR spectra of the γ-irradiated samples. NMR spectra of samples containing paramagnetic centres can become broadened or experience a shift of the resonance signal due to (i) pseudo contact shift (PCS), (ii) contact shift (CS) and (iii) paramagnetic relaxation enhancement (PRE) [47]. PCS arises from a through space, dipolar interaction between the nucleus and the unpaired electron spin which typically broaden NMR signals [48]. Figure S7, shows the ^{11}B MAS NMR spectra of the unirradiated and 25 MGy γ-irradiated samples, and illustrates the absence of apparent broadening for all compositions after γ-radiation (Figure S7) indicating that either the hyperfine coupling between ^{11}B with the unpaired electrons is not observed under the experimental conditions used or there are insufficient paramagnetic centres in the glass samples to cause any broadening due to PCS.

CS is due to the direct bond transfer (*i.e.*, spin delocalisation) of the unpaired electron onto the nucleus [47]. The CS causes the NMR resonances to shift and can be used to determine whether the unpaired electrons are delocalised onto the nucleus, resulting in a positive shift, or whether the unpaired electrons polarise a negative spin density at the nucleus, giving a negative shift [47,49]. Figure S8 shows a much larger spectral width (1000 ppm → -1000 ppm) than Figure 4 for the ^{11}B MAS NMR spectra of MW

½Li unirradiated and irradiated to 25 MGy and reveals identical spinning sidebands manifold, the absence of any additional signals outside of the isotropic resonances at ~ 15 ppm and ~ 0 ppm, and no significant shift of these resonances.

Additionally, PRE, which is driven by unpaired electron having a magnetic moment ~ 10^3 times larger than nuclear magnetic moments [50], provides more effective relaxation pathways resulting in faster nuclear spin relaxation. The ^{11}B T_1s of the BO_3 and $[BO_4]^-$ sites are obtained independently due to being resolved in the corresponding spectra which arise from their different coordinations and environments. In the unirradiated glasses, the $[BO_4]^-$ sites have a shorter T_1 than the BO_3 potentially due to the quadrupolar neighbours (^{23}Na and ^{7}Li) charge balancing the anionic site which creates more relaxation pathways resulting in enhanced signal decay. The ^{11}B T_1s of the BO_3 and $[BO_4]^-$ sites in the unirradiated and 25 MGy γ-irradiated samples are compared in Table S1 and point out to the absence of reduction in ^{11}B T_1 values induced by γ-radiation, thus suggesting that PRE effects are not experimentally observed in the borate network. This result perhaps further infers there are insufficient paramagnetic centres in the glass samples to influence the ^{11}B T_1 even when the glasses reach their defect saturation dose.

The ^{23}Na MAS NMR spectra of the unirradiated and 25 MGy γ-irradiated glass powders are compared in Figure S9 and exhibit a single broad resonance centered around -10 ppm [51,52]. The line-shapes are symmetric suggesting an even distribution of Na-O bond lengths and angles in all the glass compositions. Similarly to the ^{11}B MAS NMR spectra, no broadening due to PCS is observed in the 25 MGy γ-irradiated ^{23}Na MAS NMR spectra, suggesting that perhaps there are insufficient paramagnetic centres in the glass network to cause significant broadening. The ^{23}Na NMR spectra of MW ½Li comparing the unirradiated and 25 MGy with a larger spectral width (400 ppm → -400 ppm) is shown in Figure S10 and no additional resonances or shift of the -10 ppm signal are observed. While it might be possible that an additional resonance appears outside this the spectral width window, this result is consistent across all nuclei, and it is thus likely that there is an insufficient number of paramagnetic centres in the γ-irradiated samples and hence no changes are observed in the ^{23}Na NMR spectra due to

CS. The ^{23}Na T_1 values of the unirradiated and 25 MGy γ- irradiated samples are also given in Table S1 and indicate that no significant reduction in ^{23}Na T_1 was also observed after 25 MGy γ-radiation.

The absence of any change in the ^{11}B and ^{23}Na MAS NMR spectra caused by PCS, CS or in T_1 values induced by PRE strengthens the case that 0.1 wt% electron spin concentration (of $Cu(OAc)_2$) is insufficient for the paramagnetic species to significantly influence the glass network.

Quantitative ^{29}Si MAS NMR spectra comparing the unirradiated and 25 MGy γ-irradiated versions of the glass powders at 400 MHz are shown in Figure 5 and exhibit a single broad resonance peak centered around -100 ppm. The spectra are broad due to the amorphous nature of the glass which results in a large distribution of Si-O bond lengths and O-Si-O bond angles [53]. Silicon exists in tetrahedral coordination in the glass network denoted as Q^n, where n ranges from 0 to 4 and denotes the number of bridging oxygens surrounding the central silicon atom. The mean isotropic chemical shifts of Q^4, Q^3, and Q^2 are typically reported in the literature at -110, -95 and -85 ppm, respectively, and shows an inverse relationship between the number of bridging oxygens and chemical shift [13,52–56]. Silicon is the main network former in the MW and CaZn glass compositions therefore it will form linkages with most of the other elements in the network such as Si-O-Si, Si-O-Al, Si-O-B and Si-O-Zn [57,58]. These linkages all have overlapping chemical shift ranges which prevent their individual observation in the ^{29}Si MAS NMR spectra [52–55].

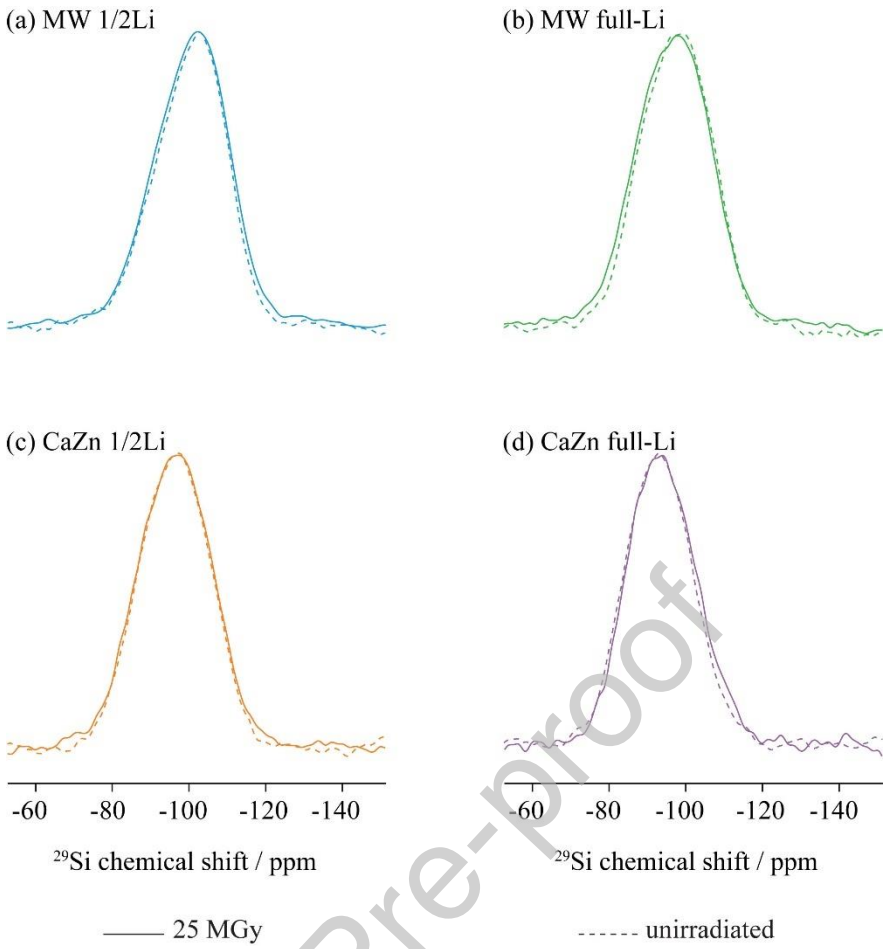

Figure 5. Experimental ^{29}Si MAS NMR spectra at 400 MHz of unirradiated (dashed) and 25 MGy γ-irradiated (solid) for (a) MW ½Li, (b) MW full-Li, (c) CaZn ½Li and (d) CaZn full-Li.

Comparison of the ^{29}Si MAS NMR spectra (Figure 5) of the 25 MGy γ-irradiated (solid lines) and unirradiated glasses (dashed lines) show negligible change in the NMR line-shapes indicating no broadening due to PCS. Additionally, the ^{29}Si NMR spectra do not exhibit any additional resonances or shifts outside the isotropic resonance for Q^n species at ~ -100 ppm, indicating that the ^{29}Si resonance does not experience an observable CS under the experimental conditions used.

To further assess potential ^{29}Si NMR signal dampening and paramagnetic bleaching due to the presence of the defect species, additional quantitative ^{29}Si MAS NMR spectra were collected on the unirradiated and 25 MGy CaZn full-Li samples under the exact same experimental conditions (using the same sample weight, number of transients and other NMR acquisition parameters, Figure S11). The NMR signal intensity of the 25 MGy sample is ~ 5 % lower that of the unirradiated one, but on the order of

noise level indicating that paramagnetic bleaching is very small, if any. As mentioned previously, the maximum electron spin concentration in the glasses after 25 MGy γ-radiation was determined to be ~ 0.1 wt% thus suggesting that there are not enough paramagnetic species in these glasses to induce PCS, CS or to cause any changes in the NMR line-shape or the connectivity of the silicate subnetwork.

Despite no observable changes in the connectivity of the silicate subnetwork due to 25 MGy γ-radiation, PRE effect is observed in ^{29}Si NMR upon γ-radiation dose (Figure 6). ^{29}Si T_1 values were determined from saturation build up curves for each composition at every γ-radiation dose and are given in Figure S12. In both ½Li compositions, the introduction of 0.5 MGy γ-radiation results in a sharp decrease in T_1 values, whereas only a small notable decrease is observed in CaZn full-Li and no change was observed in MW full-Li. This latter glass composition contains iron contamination most likely acquired during the preparation of the glass samples (Table 1) and thus already experiences PRE from paramagnetic iron shortening the ^{29}Si T_1 measured.

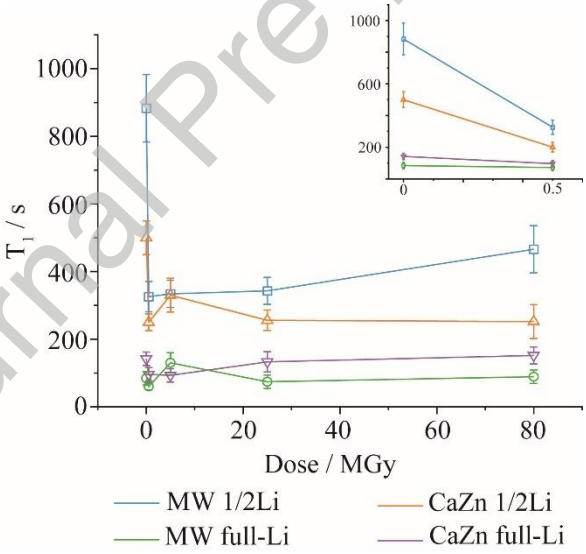

Figure 6. ^{29}Si T_1 data recorded at 400 MHz for MW ½Li (blue, squares), MW full-Li (green, circles), CaZn ½Li (orange, triangles) and CaZn full-Li (purple, inverted triangles) at all γ-radiation doses (Figure S12) and on the unirradiated samples [13]. The insert shows a comparison of the ^{29}Si T_1 data for the unirradiated and lowest irradiated samples. T_1 values were obtained from ^{29}Si saturation recovery experiments as detailed in the experimental section.

Beyond irradiation by 0.5 MGy γ, the ^{29}Si T_1s do not vary significantly with increasing γ-irradiation dose. These results indicate that no additional paramagnetic relaxation is observed suggesting that this dose is already high enough to drive the ^{29}Si T_1 relaxation pathways and introduce strong PRE.

4. Discussion

4.1 Radiation induced defects at room temperature

In the MW glass, the primary defect created upon irradiation with γ-rays are BOHCs (45 %, Table 2); the BOHC centre line-shape dominates the EPR spectra of both full and ½Li MW. It has been debated whether the hole resides on a bridging or non-bridging oxygen on the BO_3 site [59–61]. However, we have previously deduced experimentally from ^{11}B MAS NMR [13] that there are no NBOs present on the BO_3 or $[BO_4]^-$ sites in either MW and CaZn; thus, we can infer that the hole centres formed in these glass compositions are only on bridging oxygens in the boron network. Additionally, as the lithium content is increased the number of BO_3 sites and the total number of defects decreases. This confirms that the BOHC are forming on the BO_3 sites in both MW and CaZn and that lithium helps to stabilise the glass network against paramagnetic defects by transforming $BO_3 \rightarrow [BO_4]^-$. It is interesting that CaZn possesses more BO_3 sites than MW yet has a smaller number of BOHCs (45 % in MW and 25 % CaZn, Table 2). This may be due to the CaZn glass being more stable against the formation of paramagnetic defects than MW due to the presence of additional network modifiers and formers such as Ca^{2+} and Zn^{2+} which will redistribute themselves in the glass network and so balance the charges created due to ionisation by γ-rays. The large number of BOHCs in MW may also be responsible for the lower radiation tolerance of this glass composition.

The defect assigned to a HC is a hole centre on a non-bridging oxygen bonded to silicon, known as a HC_1 defect. If the oxygens here were bridging, then a hyperfine interaction involving the silicon nuclei may potentially be observed. Furthermore, from previous work [13] it was determined from ^{11}B MAS NMR experiments, for both ½ and full-Li MW and CaZn, that no NBOs were present on any of the boron sites. Thus, it can potentially be confirmed that the HC_1 defect is a hole trapped in a single orbital

of a single non-bridging oxygen bonded to one silicon atom but beyond the detection limit of ^{29}Si MAS NMR for observation.

The ET centre defect is likely caused by an electron becoming trapped on a cation, such as Li^+, Na^+ or Ca^{2+} in these glass compositions. Upon irradiation, alkali ions in the glass network can act as electron traps which may result in clustering and the formation of larger complexes. It was previously postulated that the ET centre in the MW composition was due to electrons becoming trapped on Na^+ ions resulting in the formation of metallic sodium [17]. This is one possibility, however, from the experimental data presented here the electrons could also be trapped on the Li^+ ions. When the electrons become trapped on alkali ions such as Na^+ or K^+, edges are observed in the EPR spectra [3] and the g-values are approximately half of that of a free electron ($g_0 = 2.0023$); however, in this work the g-values of the ET centre are very close to the value of a free-electron. In the experimental spectra (Figure 1) or spectral deconvolution (Figure 2), no low field peaks are observed but a high field peak is present at ~ 360 mT [4]. This component has been attributed to an impurity and is discussed in greater detail below. No peaks are observed when the electron becomes trapped on the Li^+ ion because the s-state coupling constant for lithium is smaller than sodium; thus, the electron resonance overlaps with the central hole resonance, making it indistinguishable [4]. Furthermore, as it is suggested that alkali ions tend to cluster after trapping electrons, it is expected that Li^+ ions will come together quickly and in large numbers due to the small size of the Li^+ ions and their high mobility. The agglomeration of alkali ions may result in trapped electrons to become spin-paired, rendering them non-paramagnetic. This is a possible explanation for the absence of PCS or CS in the ^{11}B, ^{23}Na and ^{29}Si NMR spectra of the glasses at the highest defect concentration. This ET centre could be due to Li^+ and Na^+ ions, however the experimental evidence and line-shape analysis suggests it is more likely to be a Li^+ ion ET centre.

The presence of E' centres after irradiation was confirmed through spectral fitting. The E' signal (highlighted in the inlet of Figure 2(c)) is due to an electron becoming trapped on an oxygen vacancy on Si Q^3. From ^{29}Si MAS NMR no change in the connectivity of the silicon network was observed thus we can potentially postulate that the γ-radiation did not result in the breaking of Si-O-Si bonds but, instead, there was potentially already an oxygen vacancy on the Si Q^3 sites resulting in an electron

becoming trapped. It was found that the concentration of E' centres decreases rapidly at room temperature with the doping of alkalis [4], possibly explaining that the increased lithium content leads to a reduction in defects in the glass compositions studied here. The ^{29}Si MAS NMR spectra indicate that the CaZn network possesses more Q^3 sites than MW resulting in a larger probability of E' centres forming. Despite this, MW and CaZn possess approximately the same percentage of E' centres (~ 10 %).

The Oxy defect centre is related to a peroxy radical bonded to silicon or aluminium in the glass network [62]. The main difference in the EPR line-shape of MW and CaZn is the dominance of this Oxy centre in CaZn, seen as a sharp signal around 350 mT in Figure 1 (c) and (d), respectively, and is thus likely due to the large number of Q^2 and Q^3 units in CaZn compared to MW [13]. While the Oxy defect is present in both the MW and CaZn networks, the nature of the defect and the g-value did not vary and as there is only a small amount of aluminium present in the MW glass (Table 1), one can assume that the Oxy defect here is associated with silicon. Furthermore, in the CaZn EPR spectra no hyperfine splitting due to aluminium (I = 5/2 for ^{27}Al that is 100% naturally abundant) is observed, therefore supporting that the Oxy defect in both MW and CaZn is not associated with aluminium and most likely linked to silicon atoms only [32,62].

The presence of Fe^{3+} ions in the MW full-Li has an impact on the total number of paramagnetic defects as Fe^{3+} acts as an electron trap where $Fe^{3+} + e^- \rightarrow Fe^{2+}$ occurs upon irradiation [63] and no known Fe^{2+} resonance is seen at room temperature [64]. This will introduce a larger error in the number of defects present in MW full-Li as there may be potential γ-radiation induced defects not observed due to the 'healing' nature of Fe^{3+} in the glass network.

The possible presence of an impurity in the both the MW and CaZn full-Li was observed from line-shape simulation of the experimental EPR spectra that shows an isotropic g component (Figure 2 (d)). Work published on sodium-barium-borosilicate glasses suggested that a radical with very similar g-values [17] (1.974 reported compared to 1.965 in this work) may be a polaron centre which is formed when an electron is trapped on a sodium cation converting it into elemental sodium. However, the authors [17] did not observe the presence of this polaron in the lithium-sodium-borosilicate glasses also

studied. This may suggest that this polaron centre is not restricted to barium-sodium borosilicate glasses as suggested by the authors but possibly exists in the MW and CaZn glasses studied here. Further work is needed to confirm whether this defect is assigned as an impurity or a possible polaron.

4.2 Defect saturation

For all glass compositions in this work, the formation of paramagnetic defects increases with dose up to 25 MGy after which saturation occurs, and the formation of defects declines when the γ-radiation dose reaches 80 MGy. This implies that the rate of ionisation dominates in the region 0-25 MGy and the rate of recombination/annihilation controls the 25-80 MGy region. This is consistent with trends relating radiation dose and defect concentration for other borosilicate glasses [65,66]. It was previously noted that for simple borosilicate glasses (containing no lithium or other elements) defects began to saturate at a γ-ray dose of around 0.1 MGy [67]. This is in sharp contrast with the work presented here that identities a saturation occurring around 25 MGy and suggests that, due to the presence of lithium, the saturation point of defect production occurs at a factor of approximately 100 times higher than those glasses without lithium. One other study noted that when borosilicate glasses are irradiated with X-ray and β-radiation the electron spin concentration of paramagnetic defects saturate at around 0.01 MGy (~ 10^{15} spin/cm^3) [68]. The authors state that this saturation likely arises from the high dose rate of > 2 x 10^3 Gy/sec used (*vs.* ~ 3 Gy/sec here in this work) which may cause radiation annealing of defects and the formation of transient defects which have a lifetime of ~ 1 ms that are also annealed under irradiation. The lower dose rate used in this work therefore suggests that the saturation of defects between 25-80 MGy in MW and CaZn is unlikely to be due to dose-rate dependant defect annealing. As the defects formed after γ-radiation are all either electron trap centres or hole centres, it is possible that defect saturation and decline occurs through the recombination of electron hole pairs.

Another possible explanation for the saturation and decline of defects between 25-80 MGy may be a result of the γ-radiation inducing further oxidation, where a two-electron oxidation state is created which would be EPR silent. However, if more defects were being created between 25-80 MGy then a change in the line-shape or shift of the ^{11}B NMR spectra on the 80 MGy versions of the glasses might be observed. However, as shown in the corresponding ^{11}B MAS NMR spectra (Figure S13) there is no

significant difference between the unirradiated and 80 MGy spectra; thus, if additional defects are formed at 80 MGy they have no impact on the boron subnetwork.

The dose rate used in this study greatly exceeds the dose rate that the 'true' high level nuclear waste glass will experience. A higher dose rate was employed due to the long irradiation times involved using available radioactive sources to cause bulk irradiation. Therefore, it is likely that the MW and CaZn glasses containing nuclear waste will not reach this saturation point as the rate of ionisation may be similar to the rate of recombination. This is a positive outcome as these results indicate that even when defect saturation is reached no change in connectivity is observed.

4.3 Effect of 25 MGy γ-irradiation on NMR spectra

The ^{11}B, ^{23}Na and ^{29}Si MAS NMR spectra of the 25 MGy γ-irradiated versions of MW and CaZn at both full and ½Li contents indicate that the network connectivity of all glass compositions remains largely unchanged when saturated with paramagnetic defects. The same quadrupolar parameters (C_Q and η) that were used to fit the ^{11}B spectra of the unirradiated versions of the glasses could be used to fit the ^{11}B spectra of the 25 MGy versions. This indicates that these parameters for the BO_3 sites remain unchanged upon network saturation saturated with γ-radiation induced defects. The magnitude of C_Q depends on the electric field gradient (EFG) at the nucleus which reflects the local symmetry of the site, thus C_Q enables insight into the coordination and distortion [69]. A larger C_Q indicates a more distorted site; thus, with the experimental results obtained here, it seems that BO_3 site distortion is not influenced by 25 MGy γ-radiation. Furthermore, the asymmetry parameter η, which influences the peak shape, also remain unchanged after 25 MGy γ-radiation. Thus, even when the glass network has been saturated with defects (at the electron spin concentration of ~ 0.1 wt% for the γ-irradiated powders determined above) the connectivity and local environment likely remain largely similar. This is an exciting result as these glass compositions have been formulated to vitrify the UK's high level nuclear waste and

indicates that 25 MGy γ-radiation will not affect the ability of the glass to immobilise components of the waste.

4.4 Effect of γ-radiation on ^{29}Si T_1

An interesting relationship between the ^{29}Si T_1s and the γ-radiation dose is obtained (Figure 6). There is a sharp, notable decrease in the ^{29}Si T_1 values for the ½Li compositions of both MW and CaZn glasses with a low dose of 0.5 MGy γ-radiation. This indicates that the formation of ET and Oxy centres created in the silicate network of the ½Li glasses results in an initial reduction in the ^{29}Si T_1 value due to paramagnetic species being introduced. Upon further γ-radiation dose, no further reduction in ^{29}Si T_1s is observed (Table S1), suggesting that no additional paramagnetic species are created in the silicate network, or that the PRE effect dominates. This result supports the hypothesis that the ET centres are forming on Li^+ ions which may cluster together at high γ-doses resulting in spin paired species. This may also explain the absence of observable changes in the ^{29}Si NMR spectra of the 25 MGy γ-irradiated glasses.

It was previously observed in the unirradiated version of these glasses that an increase in lithium content resulted in a decrease in ^{29}Si T_1s (Table S1) due to a more efficient quadrupolar relaxation mechanism between ^{7}Li (and ^{23}Na) with ^{29}Si [13]. The absence of γ-radiation induced PRE in the full lithium samples, which could suggest that defect recombination is facilitated by increased Li content further supporting the hypothesis that lithium is acting to stabilise the glass network against the formation of paramagnetic defects. Note that EPR signals that were present in the unirradiated full-Li glasses suggests that PRE may have occurred prior to γ-radiation due to potential iron contamination in both samples.

As reported above the ^{11}B and ^{23}Na T_1s did not suffer from PRE unlike ^{29}Si nuclei. This is likely due to quadrupolar nature of ^{11}B and ^{23}Na, both with S = 3/2, which dominates the relaxation. It is likely that the impact, if any, of γ-radiation on ^{11}B and ^{23}Na T_1 is overcast by quadrupolar relaxation of these

nuclei. As ^{29}Si has S = ½ it does not undergo this relaxation process, thus significant reductions of T_1 due to PRE can be observed, Table S1.

5. Conclusions

We have investigated the effect that lithium concentration has on the formation of paramagnetic defects upon γ-irradiation in 4- and 7-oxide glass networks. X-band EPR spectroscopy revealed that as more lithium is added to both the MW and CaZn networks fewer paramagnetic defects are formed. This is likely due to the transformation of $BO_3 \rightarrow [BO_4]^-$ upon lithium addition. Since the experimental evidence suggests that BOHC form on BO_3 sites, the transformation of these sites results in a reduction in the number of defects. By carrying out semi-quantitative EPR experiments, we have determined the γ-ray saturation dose to be ~ 25 MGy in all 4 glass compositions. No changes in the boron, sodium or silicon subnetworks were observed from ^{11}B, ^{23}Na and ^{29}Si MAS NMR measurements on the glass samples at this 25 MGy defect saturation point. This is perhaps due to the small percentage of paramagnetic defects in the glass network, determined to be ~ 0.1 wt%. Upon irradiation with 0.5 MGy, NMR experiments measuring the ^{29}Si T_1s revealed a relationship between lithium content, T_1 and γ-ray dose for the ½-Li glasses only. It was also found that the 7-oxide (CaZn) glass was more radiation tolerant than the 4-oxide (MW) which is attributed to the additional oxides and the lesser number of BOHCs in the former.

Supporting Information Available

Supporting information is available online as a word document.

Corresponding Authors

*****Aine G. Black: a.g.black@liverpool.ac.uk

*****Maulik K. Patel: maulik@liverpool.ac.uk

*****Frédéric Blanc: frederic.blanc@liverpool.ac.uk

Data availability

Research data supporting this work are accessible from the University of Liverpool Research Data Catalogue: (ID 8368667C-F66A-4160-8D44-0C6885836321)

Acknowledgments

The authors acknowledge the Growing Skills for Reliable Economic Energy from Nuclear (GREEN) Engineering and Physical Sciences Research (EPSRC) Centre for Doctoral Training (CDT) and the United Kingdom National Nuclear Laboratory for funding, including support of a studentship to A. G. B. under EP/S022295/1. A. S., P. A. B., L. L., M. K. P., and F. B. acknowledge, with thanks, support from EPSRC under EP/T016337/1 and for funding the 800 MHz NMR spectrometer under EP/S013393/1, respectively. The authors are very grateful to Prof. Stephen P. Brown and Dr. Anjali Menakath at the University of Warwick for providing access to the 500 MHz spectrometer and for technical support. We acknowledge the support of The University of Manchester's Dalton Cumbrian Facility (DCF), a partner in the National Nuclear User Facility, the EPSRC UK National Ion Beam Centre and the Henry Royce Institute. We thank EPSRC for funding the National Research Facility for EPR Spectroscopy (EP/W014521/1 and EP/V035231/1) at The University of Manchester. A. B. and M. S. also thank EPSRC and The University of Manchester for the financial support.

References

[1] M.I. Ojovan, W.E. Lee, S.N. Kalmykov, An introduction to nuclear waste immobilisation, Elsevier, 2019. https://doi.org/10.1016/C2017-0-03752-7.

[2] S. Gin, P. Jollivet, M. Tribet, S. Peuget, S. Schuller, Radionuclides containment in nuclear glasses: an overview, Radiochim. Acta. 105 (2017) 927–959. https://doi.org/10.1515/ract-2016-2658.

[3] D.L. Griscom, ESR and optical studies of alkali-associated trapped-electron centres in alkali

borate glass irradiated at 77°K*, J. Non. Cryst. Solids. 6 (1971) 275–282.

[4] D.L. Griscom, E.S.R. studies of radiation damage and structure in oxide glasses not containing transition group ions: A contemporary overview with illustrations from the alkali borate system, J. Non. Cryst. Solids. 13 (1974) 251–285. https://doi.org/10.1016/0022-3093(74)90095-7.

[5] D.. Griscom, Electron spin resonance studies of trapped hole centers in irradiated alkali silicate glasses: A critical comment on current models for HC1 and HC2, J. Non. Cryst. Solids. 64 (1984) 229–247. https://doi.org/10.1016/0022-3093(84)90220-5.

[6] D.L. Griscom, C.I. Merzbacher, R.A. Weeks, R.A. Zuhr, Electron spin resonance studies of defect centers induced in a high-level nuclear waste glass simulant by gamma-irradiation and ion-implantation, J. Non. Cryst. Solids. 258 (1999) 34–47. https://doi.org/10.1016/S0022-3093(99)00557-8.

[7] S. Gin, A. Abdelouas, L.J. Criscenti, W.L. Ebert, K. Ferrand, T. Geisler, M.T. Harrison, Y. Inagaki, S. Mitsui, K.T. Mueller, J.C. Marra, C.G. Pantano, E.M. Pierce, J. V. Ryan, J.M. Schofield, C.I. Steefel, J.D. Vienna, An international initiative on long-term behavior of high-level nuclear waste glass, Mater. Today. 16 (2013) 243–248. https://doi.org/10.1016/j.mattod.2013.06.008.

[8] T. Famprikis, P. Canepa, J.A. Dawson, M.S. Islam, C. Masquelier, Fundamentals of inorganic solid-state electrolytes for batteries, Nat. Mater. 18 (2019) 1278–1291. https://doi.org/10.1038/s41563-019-0431-3.

[9] M. Li, J. Lu, Z. Chen, K. Amine, 30 Years of Lithium-Ion Batteries, Adv. Mater. 30 (2018) 24. https://doi.org/10.1002/adma.201800561.

[10] A. Bunde, K. Funke, M.D. Ingram, Ionic glasses: History and challenges, Solid State Ionics. 105 (1998) 1–13. https://doi.org/10.1016/s0167-2738(97)00444-x.

[11] C. Calahoo, L. Wondraczek, Ionic glasses: Structure, properties and classification, J. Non-

Crystalline Solids X. 8 (2020) 100054. https://doi.org/10.1016/j.nocx.2020.100054.

[12] C.M. Jantzen, W.E. Lee, M.I. Ojovan, Radioactive waste (RAW) conditioning, immobilization, and encapsulation processes and technologies: overview and advances, in: Radioact. Waste Manag. Contam. Site Clean-Up, Elsevier, 2013: pp. 171–272. https://doi.org/10.1533/9780857097446.1.171.

[13] A.G. Black, A. Scrimshire, D. Iuga, Y. Lavallée, K.A. Morrison, P.A. Bingham, T. Taylor, L. Leay, M.T. Harrison, F. Blanc, M.K. Patel, Effect of lithium concentration on the network connectivity of nuclear waste glasses, J. Non. Cryst. Solids. 646 (2024) 123234. https://doi.org/10.1016/j.jnoncrysol.2024.123234.

[14] G. Tricot, J. Trébosc, F. Pourpoint, R. Gauvin, L. Delevoye, The D-HMQC MAS-NMR Technique: An Efficient Tool for the Editing of Through-Space Correlation Spectra Between Quadrupolar and Spin-1/2 (^{31}P, ^{29}Si, ^{1}H, ^{13}C) Nuclei, 1st ed., Elsevier Ltd., 2014. https://doi.org/10.1016/B978-0-12-800185-1.00004-8.

[15] D. Iuga, C. Morais, Z. Gan, D.R. Neuville, L. Cormier, D. Massiot, NMR heteronuclear correlation between quadrupolar nuclei in solids, J. Am. Chem. Soc. 127 (2005) 11540–11541. https://doi.org/10.1021/ja052452n.

[16] N.A. Brown, Understanding The Effect of Ionising Radiation on The Properties of Vitrified Nuclear Waste, University of Manchester, 2023.

[17] P. Rautiyal, G. Gupta, R. Edge, L. Leay, A. Daubney, M.K. Patel, A.H. Jones, P.A. Bingham, Gamma irradiation-induced defects in borosilicate glasses for high-level radioactive waste immobilisation, J. Nucl. Mater. 544 (2021) 152702. https://doi.org/10.1016/j.jnucmat.2020.152702.

[18] O.J. McGann, P.A. Bingham, R.J. Hand, A.S. Gandy, M. Kavčič, M. Žitnik, K. Bučar, R. Edge, N.C. Hyatt, The effects of γ-radiation on model vitreous wasteforms intended for the disposal of intermediate and high level radioactive wastes in the United Kingdom, J. Nucl.

Mater. 429 (2012) 353–367. https://doi.org/10.1016/j.jnucmat.2012.04.007.

[19] P. Rautiyal, Radiation damage effects on the structure and properties of radioactive waste glasses, Sheffield Hallam University, 2021. http://shura.shu.ac.uk/28913/.

[20] J.A.C. Marples, The preparation, properties, and disposal of vitrified high level waste from nuclear fuel reprocessing, Glas. Technol. 29 (1988) 230–247.

[21] M.T. Harrison, Vitrification of High Level Waste in the UK, Procedia Mater. Sci. 7 (2014) 10–15. https://doi.org/10.1016/j.mspro.2014.10.003.

[22] M.T. Harrison, The Effect of Composition on Short- and Long-term Durability of UK HLW Glass, Procedia Mater. Sci. 7 (2014) 186–192. https://doi.org/10.1016/j.mspro.2014.10.025.

[23] L. Leay, W. Bower, G. Horne, P. Wady, A. Baidak, M. Pottinger, M. Nancekievill, A.D. Smith, S. Watson, P.R. Green, B. Lennox, J.A. Laverne, S.M. Pimblott, Development of irradiation capabilities to address the challenges of the nuclear industry, Nucl. Instruments Methods Phys. Res. Sect. B Beam Interact. with Mater. Atoms. 343 (2015) 62–69. https://doi.org/10.1016/j.nimb.2014.11.028.

[24] L. Leay, A. Baidak, C. Anderson, C.M. Chan, A. Daubney, T. Donoclift, G. Draper, R. Edge, J. Hobbs, L. Jones, N.J.S. Mason, D. Messer, M. O'leary, R. Orr, S.M. Pimblott, S. de M. Shubeita, A.D. Smith, H. Steele, P. Wady, F. Currell, Resurgence of a nation's radiation science driven by its nuclear industry needs, Appl. Sci. 11 (2021). https://doi.org/10.3390/app112311081.

[25] D. Cordischi, M. Occhiuzzi, R. Dragone, Quantitative EPR spectroscopy: Comparison between primary standards and application to MgO-MnO and α-Al2O3-Cr2O3 solid solutions, Appl. Magn. Reson. 16 (1999) 427–445. https://doi.org/10.1007/BF03161929.

[26] G.R. Eaton, S.S. Eaton, D.P. Barr, R.T. Weber, Quantitative EPR, Springer Vienna, Vienna, 2010. https://doi.org/10.1007/978-3-211-92948-3.

[27] H. Kamat, F. Wang, K.E. Barnsley, J. V. Hanna, A.M. Tyryshkin, A. Goel, Insight into the

Partitioning and Clustering Mechanism of Rare-Earth Cations in Alkali Aluminoborosilicate Glasses, Chem. Mater. 33 (2021) 7944–7963. https://doi.org/10.1021/acs.chemmater.1c01352.

[28] D. Massiot, F. Fayon, M. Capron, I. King, S. Le Calve, B. Alonso, J.-O. Durand, B. Bujoli, Z. Gan, G. Hoatson, Modelling one- and two-dimensional solid-state NMR spectra, Magn. Reson. Chem. 40 (2002) 70–76.

[29] E. Lippmaa, M. Mági, A. Samoson, M. Tarmak, G. Engelhardt, Investigation of the Structure of Zeolites by Solid-State High-Resolution ^{29}Si NMR Spectroscopy, J. Am. Chem. Soc. 103 (1981) 4992–4996. https://doi.org/10.1021/ja00407a002.

[30] M. Mohapatra, R.M. Kadam, R.K. Mishra, C.P. Kaushik, B.S. Tomar, S. V. Godbole, Gamma Radiation-Induced Changes in Trombay Nuclear Waste Glass Containing Iron, Int. J. Appl. Glas. Sci. 4 (2013) 53–60. https://doi.org/10.1111/j.2041-1294.2012.00094.x.

[31] T.T. Wang, X.Y. Zhang, M.L. Sun, X. Du, M. Guan, H.B. Peng, T.S. Wang, γ-Irradiation effects in borosilicate glass studied by EPR and UV–Vis spectroscopies, Nucl. Instruments Methods Phys. Res. Sect. B Beam Interact. with Mater. Atoms. 464 (2020) 106–110. https://doi.org/10.1016/j.nimb.2019.12.007.

[32] B. Boizot, G. Petite, D. Ghaleb, G. Calas, Radiation induced paramagnetic centres in nuclear glasses by EPR spectroscopy, Nucl. Instruments Methods Phys. Res. Sect. B Beam Interact. with Mater. Atoms. 141 (1998) 580–584. https://doi.org/10.1016/S0168-583X(98)00102-5.

[33] R.A. Weeks, Paramagnetic Resonance of Lattice Defects in Irradiated Quartz, J. Appl. Phys. 27 (1956) 1376–1381. https://doi.org/10.1063/1.1722267.

[34] D. Goldfarb, S. Stoll, EPR spectroscopy : fundamentals and methods, Wiley, Chichester, West Sussex, England, 2018.

[35] D.A. Dutt, P.L. Higby, D.L. Griscom, An electron spin resonance study of X-irradiated calcium aluminosilicate glasses, J. Non. Cryst. Solids. 130 (1991) 41–51. https://doi.org/10.1016/0022-3093(91)90154-X.

[36] E.J. Friebele, D.L. Griscom, M. Stapelbroek, R.A. Weeks, Fundamental Defect Centers in Glass: The Peroxy Radical in Irradiated, High-Purity, Fused Silica, Phys. Rev. Lett. 42 (1979) 1346–1349. https://doi.org/10.1103/PhysRevLett.42.1346.

[37] H. Hosono, Y. Abe, Photosensitivity and structural defects in dopant-free ultraviolet-sensitive calcium aluminate glasses, J. Non. Cryst. Solids. 95–96 (1987) 717–724. https://doi.org/10.1016/S0022-3093(87)80673-7.

[38] D.T. Petasis, EPR Spectroscopy, De Gruyter, 2022. https://doi.org/10.1515/9783110417562.

[39] S. Agnello, L. Nuccio, Thermal stability of gamma-irradiation-induced oxygen-deficient centers in silica, Phys. Rev. B - Condens. Matter Mater. Phys. 73 (2006) 1–6. https://doi.org/10.1103/PhysRevB.73.115203.

[40] P. Martín, M. León, A. Ibarra, E.R. Hodgson, Thermal stability of gamma irradiation induced defects for different fused silica, J. Nucl. Mater. 417 (2011) 818–821. https://doi.org/10.1016/j.jnucmat.2010.12.171.

[41] L.S. Du, J.F. Stebbins, Site preference and Si/B mixing in mixed-alkali borosilicate glasses: A high-resolution ^{11}B and ^{17}O NMR study, Chem. Mater. 15 (2003) 3913–3921. https://doi.org/10.1021/cm034427r.

[42] F. Angeli, O. Villain, S. Schuller, T. Charpentier, D. De Ligny, L. Bressel, L. Wondraczek, Effect of temperature and thermal history on borosilicate glass structure, Phys. Rev. B - Condens. Matter Mater. Phys. 85 (2012) 1–15. https://doi.org/10.1103/PhysRevB.85.054110.

[43] P.M. Aguiar, S. Kroeker, Boron speciation and non-bridging oxygens in high-alkali borate glasses, J. Non. Cryst. Solids. 353 (2007) 1834–1839. https://doi.org/10.1016/j.jnoncrysol.2007.02.013.

[44] F. Angeli, T. Charpentier, M. Gaillard, P. Jollivet, Influence of zirconium on the structure of pristine and leached soda-lime borosilicate glasses: Towards a quantitative approach by ^{17}O MQMAS NMR, J. Non. Cryst. Solids. 354 (2008) 3713–3722.

https://doi.org/10.1016/j.jnoncrysol.2008.03.046.

[45] T.L. Goût, M.T. Harrison, I. Farnan, Impacts of lithium on Magnox waste glass dissolution, J. Non. Cryst. Solids. 517 (2019) 96–105. https://doi.org/10.1016/j.jnoncrysol.2019.04.040.

[46] L.S. Du, J.F. Stebbins, Solid-state NMR study of metastable immiscibility in alkali borosilicate glasses, J. Non. Cryst. Solids. 315 (2003) 239–255. https://doi.org/10.1016/S0022-3093(02)01604-6.

[47] A.J. Pell, G. Pintacuda, C.P. Grey, Paramagnetic NMR in solution and the solid state, Prog. Nucl. Magn. Reson. Spectrosc. 111 (2019) 1–271. https://doi.org/10.1016/j.pnmrs.2018.05.001.

[48] H.M. McConnell, R.E. Robertson, Isotropic Nuclear Resonance Shifts, J. Chem. Phys. 29 (1958) 1361–1365. https://doi.org/10.1063/1.1744723.

[49] F.H. Köhler, O. Storcheva, Paramagnetic Prussian Blue Analogues CsMII[MIII(CN)6]. The Quest for Spin on Cesium Ions by Use of 133Cs MAS NMR Spectroscopy, Inorg. Chem. 54 (2015) 6801–6806. https://doi.org/10.1021/acs.inorgchem.5b00711.

[50] R. Sharp, L. Lohr, J. Miller, Paramagnetic NMR relaxation enhancement: recent advances in theory, Prog. Nucl. Magn. Reson. Spectrosc. 38 (2001) 115–158. https://doi.org/10.1016/S0079-6565(00)00034-0.

[51] S.K. Lee, J.F. Stebbins, The distribution of sodium ions in aluminosilicate glasses: A high-field Na-23 MAS and 3Q MAS NMR study, Geochim. Cosmochim. Acta. 67 (2003) 1699–1709. https://doi.org/10.1016/S0016-7037(02)00026-7.

[52] T. Charpentier, S. Ispas, M. Profeta, F. Mauri, C.J. Pickard, First-Principles Calculation of ^{17}O, ^{29}Si, and ^{23}Na NMR Spectra of Sodium Silicate Crystals and Glasses, J. Phys. Chem. B. 108 (2004) 4147–4161. https://doi.org/10.1021/jp0367225.

[53] E. Schneider, J.F. Stebbins, A. Pines, Speciation and local structure in alkali and alkaline earth silicate glasses: Constraints from ^{29}Si NMR spectroscopy, J. Non. Cryst. Solids. 89 (1987)

371–383. https://doi.org/10.1016/S0022-3093(87)80279-X.

[54] M.C. Davis, D.C. Kaseman, S.M. Parvani, K.J. Sanders, P.J. Grandinetti, D. Massiot, P. Florian, $Q^{(n)}$ species distribution in $K_2O.2SiO_2$ glass by ^{29}Si magic angle flipping NMR, J. Phys. Chem. A. 114 (2010) 5503–5508. https://doi.org/10.1021/jp100530m.

[55] T. Nanba, M. Nishimura, Y. Miura, A theoretical interpretation of the chemical shift of ^{29}Si NMR peaks in alkali borosilicate glasses, Geochim. Cosmochim. Acta. 68 (2004) 5103–5111. https://doi.org/10.1016/j.gca.2004.05.042.

[56] R. Martens, W. Müller-Warmuth, Structural groups and their mixing in borosilicate glasses of various compositions - an NMR study, J. Non. Cryst. Solids. 265 (2000) 167–175. https://doi.org/10.1016/S0022-3093(99)00693-6.

[57] A. Krishnamurthy, V.K. Michaelis, S. Kroeker, Network Formation in Borosilicate Glasses with Aluminum or Gallium: Implications for Nepheline Crystallization, J. Phys. Chem. C. 125 (2021) 8815–8824. https://doi.org/10.1021/acs.jpcc.1c01262.

[58] N.J. Cassingham, M.C. Stennett, P.A. Bingham, N.C. Hyatt, G. Aquilanti, The Structural Role of Zn in Nuclear Waste Glasses, Int. J. Appl. Glas. Sci. 2 (2011) 343–353. https://doi.org/10.1111/j.2041-1294.2011.00067.x.

[59] M.C.R. Symons, Structure of Trapped-Hole Centers in γ-Irradiated Borate Glasses, J. Chem. Phys. 53 (1970) 468–469. https://doi.org/10.1063/1.1673822.

[60] D.L. Griscom, P.C. Taylor, P.J. Bray, Reply to "Structure of Trapped-Hole Centers in γ-Irradiated Borate Glasses," J. Chem. Phys. 53 (1970) 469–471. https://doi.org/10.1063/1.1673823.

[61] P.C. Taylor, D.L. Griscom, Toward a Unified Interpretation of ESR Trapped-Hole Centers in Irradiated Borate Compounds and Glasses, J. Chem. Phys. 55 (1971) 3610–3611. https://doi.org/10.1063/1.1676630.

[62] A. Le Gac, B. Boizot, C. Jégou, S. Peuget, Aluminosilicate glasses structure under electron

irradiation: An EPR study, Nucl. Instruments Methods Phys. Res. Sect. B Beam Interact. with Mater. Atoms. 407 (2017) 203–209. https://doi.org/10.1016/j.nimb.2017.06.025.

[63] F.Y. Olivier, B. Boizot, D. Ghaleb, G. Petite, Raman and EPR studies of β-irradiated oxide glasses: The effect of iron concentration, J. Non. Cryst. Solids. 351 (2005) 1061–1066. https://doi.org/10.1016/j.jnoncrysol.2005.01.018.

[64] P.A. Bingham, The Environment of Iron in Silicate Glasses, University of Sheffield, 2000.

[65] N. Ollier, R. Planchais, B. Boizot, EPR study of Yb-doped irradiated glasses, Nucl. Instruments Methods Phys. Res. Sect. B Beam Interact. with Mater. Atoms. 266 (2008) 2854–2858. https://doi.org/10.1016/j.nimb.2008.03.129.

[66] V. Gancheva, N.D. Yordanov, Y. Karakirova, EPR investigation of the gamma radiation response of different types of glasses, Spectrochim. Acta Part A Mol. Biomol. Spectrosc. 63 (2006) 875–878. https://doi.org/10.1016/j.saa.2005.10.019.

[67] S.K. Zhu, Y.Q. Sun, Y.H. Pan, X. Chen, K. Bai, Y.C. Wang, F. Yang, K.M. Qin, J.J. Mao, X.Y. Zhang, T.S. Wang, H.B. Peng, Radiation effects of B depletion and the generation of point defects in ternary borosilicate glasses by gamma rays, J. Non. Cryst. Solids. 619 (2023) 122576. https://doi.org/10.1016/j.jnoncrysol.2023.122576.

[68] B. Boizot, G. Petite, D. Ghaleb, G. Calas, Dose, dose rate and irradiation temperature effects in β-irradiated simplified nuclear waste glasses by EPR spectroscopy, J. Non. Cryst. Solids. 283 (2001) 179–185. https://doi.org/10.1016/S0022-3093(01)00338-6.

[69] S. Kroeker, Nuclear Magnetic Resonance Spectroscopy of Glasses, in: Mod. Glas. Charact., Wiley, 2015: pp. 1–30. https://doi.org/10.1002/9781119051862.ch8.

Declaration of interests

☒ The authors declare that they have no known competing financial interests or personal relationships that could have appeared to influence the work reported in this paper.

☐ The authors declare the following financial interests/personal relationships which may be considered as potential competing interests: